CHAPTER 6

DIFFERENTIAL SCANNING CALORIMETRIC STUDIES OF SEVERAL COMPOUNDS SHOWING ORDER-DISORDER TRANSITION

ABSTRACT

In this Chapter phase transition behavior of CuI, CuBr, AgI, Ag_2S, $NaNO_2$, $NaNO_3$ and KSCN have been investigated. All of them exhibit order-disorder transitions. Thermal hysteresis exhibited by these compounds have been examined in the light of their change in unit cell volumes.

INTRODUCTION

This Chapter deals with order-disorder transitions in some materials. Perfect ordering of atoms or ions in a solid can occur only when there is no thermal agitation in the molecules, that is, at OK. It is more appropriate, therefore, to describe the phenomenon in terms of the extent of order or disorder occuring. In an order-disorder transition the order parameter approaches close to zero at the transition temperature. There are three principal kinds of order-disorder transitions[1,2], viz. positional, orientational and the one involving electronic or nuclear spin states. We shall be concerned here with the positional and orientational disorderings.

Positional disordering can take place either due to the occupation of atoms or ions at the inappropriate positions of sublattice, or when there are more number of available positions for atoms or ions than are required. Orientational disordering occurs when a polyatomic ion occupying the lattice positions can exist in more than one orientation.

An order-disorder transition often occurs in the manner of lambda transition. However, it may also take place as a first order transition involving a change in volume.

Many order-disorder transitions begin as lambda transition but terminate as first order transitions.[1]

The increase in entropy in order-disorder transitions is mainly configurational in origin, and is given by the relation

$$\Delta S = R \ln (w_2/w_1) \qquad \ldots (6.1)$$

where w_2 and w_1 are the number of configurations in the disordered and ordered states, respectively.

In the case of positional disordering, the long range order parameter (LRO) vanishes when the disorder sets in, and the short range order parameter (SRO) comes into play. In most of the transitions the SRO persists even beyond the transition temperature, T_c, and the equilibrium value of LRO is not attained immediately on bringing the material to the appropriate temperature[1]. Thus the profile of a measured property which is dependent on disorder will have different characteristics as a function of time or temperature during heating and cooling. The rate at which the full value of the disorder or order is attained is generally different in the two directions. If the phenomenon is treated on the basis of first order kinetics[3] it may be shown that

$$\ln \frac{Q_f - Q_o}{Q_f - Q_t} = \frac{\hat{\tau}}{t} \qquad \ldots (6.2)$$

In this relation Q_0, Q_t and Q_f refer to the quantities measured initially, at a time t and the full value, respectively, and τ is the relaxation time. It should be pointed out that this is rather an over-simplified approach. Many models of varying rigor are discussed in the literature[4]. In many cases more than one relaxation time parameter is needed to treat the kinetics of order-disorder transitions. It may also be pointed out that relaxation time for ordering is very sensitive to temperature and its value decrease as the temperature approaches T_c; the relaxation time exhibits a minimum in the region close to and below T_c.

Kinetic studies of positional disordering are confined mostly to alloy systems. Two important points have emerged from these studies, viz. (a) the rates of disordering are much faster than ordering[5] and (b) positional ordering transitions exhibit the phenomenon of "critical slowing down"[4,5].

We have examined here the positional order-disorder transitions in CuI, CuBr, AgI and Ag_2S. Three more compounds KSCN, $NaNO_2$ and $NaNo_3$ which are known to undergo orientational order-disorder[1,2] transitions have also been investigated. Table 6.1 summarizes the crystallographic and relevant other informations for CuI, CuBr, AgI and Ag_2S; similar characteristics of KSCN, $NaNO_2$ and $NaNO_3$ are cataloged in Table 6.2.

Table 6.1

Crystallographic and relevant other data for CuI, CuBr, AgI and Ag_2S

Compound	Remarks	Reference
CuI	There are three phases for CuI. The γ -phase has ZnS structure; a = 6.032 Å at 80K and 6.114 Å at 638K has fcc lattice (space group T_d^2-F43m). The β -phase is hexagonal (ZnO type); a = 4.300 Å and c = 7.207 Å; space group D_{3h}^1. The α -phase is bcc; a = 6.158 Å; space group O_h^5. The $\gamma \longrightarrow \beta$ transition occurs at 642K; $\Delta H_{\gamma \longrightarrow \beta}$ = 1.70 kcal mol^{-1}; $\Delta S_{\gamma \longrightarrow \beta}$ = 2.64 e.u. mol^{-1}. The $\beta \longrightarrow \alpha$ transition occurs at 680K; $\Delta H_{\beta \longrightarrow \alpha}$ = 0.77 kcal mol^{-1}; $\Delta S_{\beta \longrightarrow \alpha}$ = 1.13 e.u. mol^{-1}. The $\beta \longrightarrow \alpha$ transition is order-disorder type.	6-11
CuBr	Similar to CuI there are three phases for CuBr. γ -CuBr is fcc with a = 5.6794 Å at 293K; like γ -CuI it has	8,9,12,13

contd..

Table 6.1(contd)

Compound	Remarks	Reference
	ZnS structure. β-CuBr is hexagonal; space group C_{6v}^4; a = 4.04 Å, c = 6.58 Å at ~ 703K. The $\gamma \rightarrow \beta$ transition occurs at 668K; $\Delta H_{\gamma \rightarrow \beta} = 1.4$ kcal mol^{-1}; $\Delta S_{\gamma \rightarrow \beta} = 2.1$ e.u. mol^{-1}. The β phase is bcc and is similar to AgI; space group O_h^9; a = 4.53 Å at ~ 753K. The $\beta \rightarrow \alpha$ transition occurs at 742K. $\Delta H_{\beta \rightarrow \alpha} = 0.7$ kcal mol^{-1}; $\Delta S_{\beta \rightarrow \alpha} =$ 0.9 e.u. mol^{-1}.	
AgI	Of the three AgI phases (γ, β and α) at atmospheric pressure the β-phase (wurtzite structure) is more stable than γ-phase (ZnS structure) below 420K. The $\gamma \rightarrow \beta$ transition is probably an athermal higher order	9, 13-18

contd..

Table 6.1(contd)

Compound	Remarks	Reference
	transition; $H \sim 0.1$ kcal mol^{-1}. The β-phase is hexagonal; space group C_{6v}^4 ($C6_{mc}$); $a = 4.580$ Å, $c = 7.494$ Å. The α-phase is bcc with space group $Im3m$ (O_h^9); $a = 5.068$ Å; Ag^+ ion are disordered and are distributed over 42 crystallographic sites. The $\beta \rightarrow \alpha$ transition occurs at 420K. $\Delta H_{\beta \rightarrow \alpha} = 1.53$ kcal mol^{-1}; $\Delta S_{\beta \rightarrow \alpha} = 3.6$ e.u. mol^{-1}.	
Ag_2S	There are two phases for Ag_2S. The β-phase is monoclinic; $a = 4.23$ Å, $b = 6.91$ Å, $c = 7.87$ Å, $\beta = 99^\circ 35'$; space group C_{2h}^5 ($P2_{1/m}$). The α-phase is isostructural to α-AgI; $a = 4.89$ Å. The $\beta \rightarrow \alpha$ transition occurs at 450 K. $\Delta H_{\beta \rightarrow \alpha} = 0.96$ kcal mol^{-1}; $\Delta S_{\beta \rightarrow \alpha} = 2.1$ e.u. mol^{-1}.	19-21

Table 6.2

Crystallographic and phase transition behavior of $NaNO_2$, $NaNO_3$ and KSCN

Compound	Remarks	Reference
$NaNO_2$	The room temperature phase (γ) is orthorhombic, a = 3.570 Å, b = 5.578 Å, c = 5.390 Å at 299K; space group C_{2v}^{20} (Im2m). The high temperature phase (α) is also orthorhombic; a = 3.69 Å, b = 5.68 Å, c = 5.33 Å; space group V_h^{25}(Immm). The γ-phase is ferroelectric and the α-phase is paraelectric. A first order transformation of the γ-phase occurs at 438K, and an antiferroelectric phase (β) has been reported to exist in the narrow temperature range of 436.8-438 K. $\Delta H_{\gamma \rightarrow \alpha}$ = 0.53 kcal mol^{-1}; $\Delta S_{\gamma \rightarrow \alpha}$ = 1.26 e.u. mol^{-1}. In addition to $\gamma \longrightarrow \beta \longrightarrow \alpha$ transitions, anomalies have been reported to occur at 375, 451, 488 K. Another low temperature phase (δ) has been reported at 178 K. All these transitions appear to be due order-disorder process of the NO_2 dipoles.	22-28

contd..

Table 6.2(contd)

Compound	Remarks	Reference
$NaNO_3$	There are two phases for $NaNO_3$. The room temperature phase (β) is ordered rhombohedral; a = 6.325 Å, α = $47^{\circ}16'$ at 296K. The high temperature phase (α) is disorderd rhombohedral; a = 6.56 Å, $\alpha = 45^{\circ}35'$ at 553K. The $\beta \longrightarrow \alpha$ transition (λ-type) occurs at 548.5 K. $\Delta H_{\beta \rightarrow \alpha} = 1.03$ kcal mol^{-1}.	29-32
KSCN	At room temperature KSCN has the orderd orthorhombic structure (β). The β-phase is antiferroelectric and transforms to the paraelectric α-phase (λ-type transition) at 413K. Orthorhombic β-phase; a = 6.66 Å, b = 7.58 Å, c = 6.63 Å; space group D_{2h}^{11}-Pcmb. Tetragonal α-phase; a = 6.70 Å, c = 7.73 Å; space group D_{4h}^{18}- I_4-mcm. $\Delta H_{\beta \rightarrow \alpha} = 0.529$ kcal mol^{-1}; $\Delta S_{\beta \rightarrow \alpha} = 1.30$ e.u. mol^{-1}.	33-37

EXPERIMENTAL SECTION

Materials

CuBr was prepared by the reduction of an aqueous solution of $CuCl_2 \cdot 2H_2O$ with Na_2SO_3 in accordance with the method of Keller and Wycoff[38]. The white crystalline material thus obtained was dried *in vacuo* at 80°C. The material can be preserved indefinitely if stored dry.

CuI was obtained by reacting $CuSO_4$ with KI and $Na_2S_2O_3$ in aqueous solution as described by Kauffman and Pinnel[39]. The CuI that precipitates in microcrystalline form was separated from the solution with some difficulty. The product was thoroughly washed with water and then dried *in vacuo*. However, x-ray powder photograph of this material revealed the presence of occluded $Na_2S_2O_3$[40]. The material, therefore, was dissolved in aqueous HI (Baker, 47-51 %); undissolved material was separated by filtration with a sintered glass crucible (G-4). Water was added slowly to the filtrate while stirring until the precipitation of the CuI was complete. The CuI settled readily and was separated by and washed on a glass frit. Washing with water was continued until the filtrate was acid-free. Finally three washings with dry acetone were made; the material was then dried in a vacuum oven at 100°C for 12h.

AgI was prepared according to a standard method. AgI of proper stoichiometry is obtained only when the precipitation is carried out from dilute solution in subdued light. AgI was therefore precipitated by adding a 0.05M solution of $AgNO_3$ slowly and with constant stirring to a dilute ammoniacal solution of KI until precipitation was complete, and then adding 1% HNO_3 by volume excess. The precipitate was collected on a glass frit (G-4), washed with 1% HNO_3, and finally with little water to remove nitric acid. The compound was dried in air oven at 110°C for 2h.

Ag_2S was precipitated from ammoniacal $AgNO_3$ solution (0.01M) by passing pure H_2S gas through the solution for 1h at ambient temperature. After completion of precipitation, the black Ag_2S was filtered off and washed several times with water and dried at 150°C in a stream of CO_2. This was then heated at 350°C for 1h in a stream of H_2 gas to remove excess of sulfur.

$NaNO_2$, $NaNO_3$, KSCN were all E. Merck (Darmstadt) "guranteed reagent quality" and used as obtained.

DSC measurements

For each of the specimens DSC measurements were carried out in replicate at varying heating rates. The enthalpy changes reported are the average value of at least three independent measurements.

RESULTS AND DISCUSSION

The purpose of examining the thermal behavior of the compounds under consideration have been three fold. These are: (i) To determine accurately the heats of phase transformation in the forward and reverse direction. (ii) To examine the profile of the DSC thermograms at the transition temperature in the heating and cooling cycles, that is, to see whether the disordering and ordering processes occur at the same span of temperature. (iii) To find whether the width of thermal hysteresis can be related to change in volume of the unit cells.

The heating and cooling thermograms of all the compounds under identical heating/cooling condition (1.25°C) are shown in Figures 6.1-6.7; CuI(6.1), CuBr(6.2), AgI(6.3), Ag_2S(6.4), $NaNO_2$(6.5), $NaNO_3$(6.6), KSCN (6.7). Table 6.3 summarizes the temperatures for initiation (T_i), maximum transformation (T_m) and completion (T_f) of phase transition in the heating and cooling cycles.

Inspection of the Figures 6.1-6.7 and the column Table 6.3 illustrating the span of temperature (T_f-T_i) at which a transition occurs in the forward (disordering) and reverse direction (ordering) reveal that the magnitude of (T_f-T_i) in the cooling curves is somewhat greater than the heating curves.

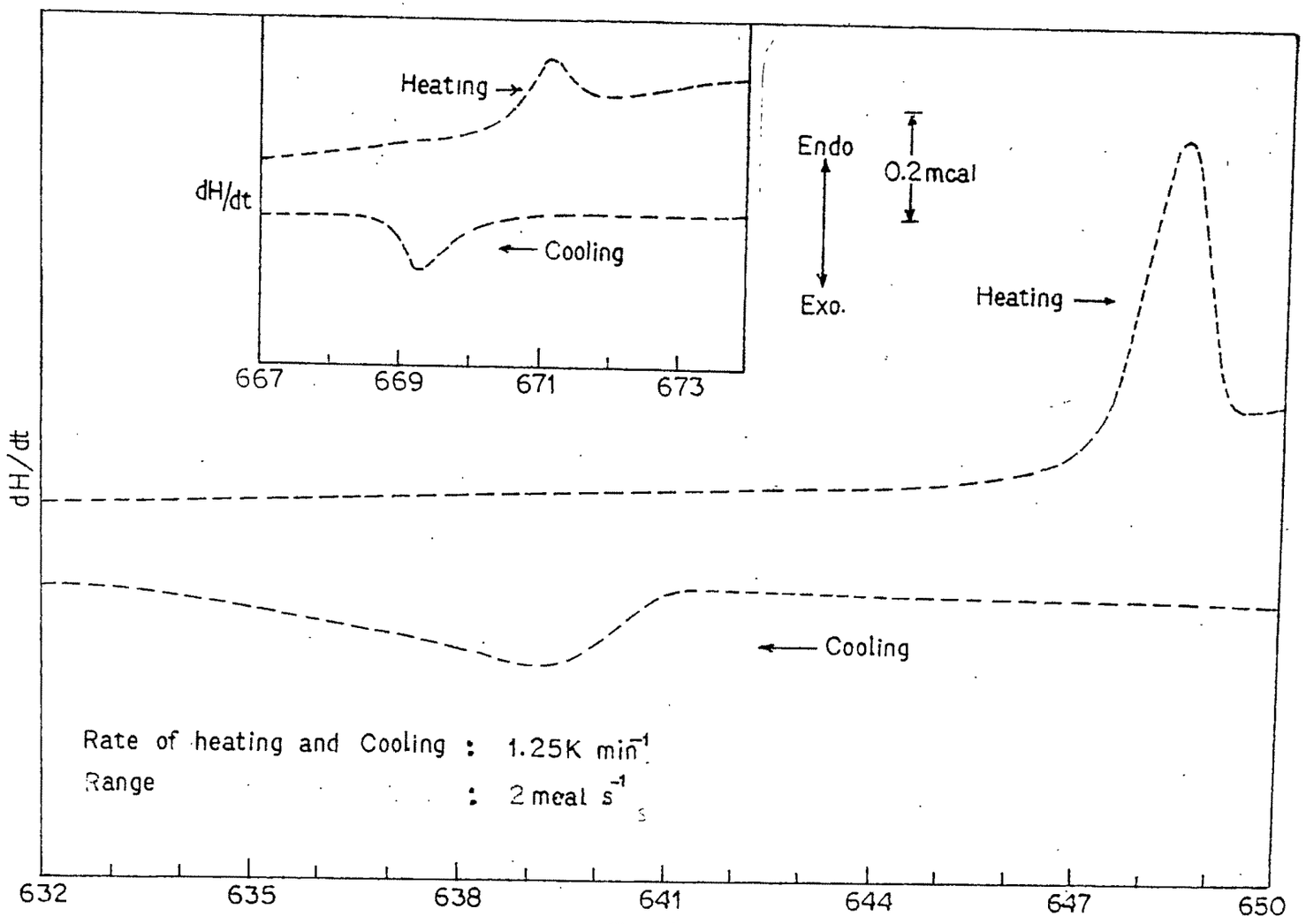

DSC scan of CuI
Figure 6.1

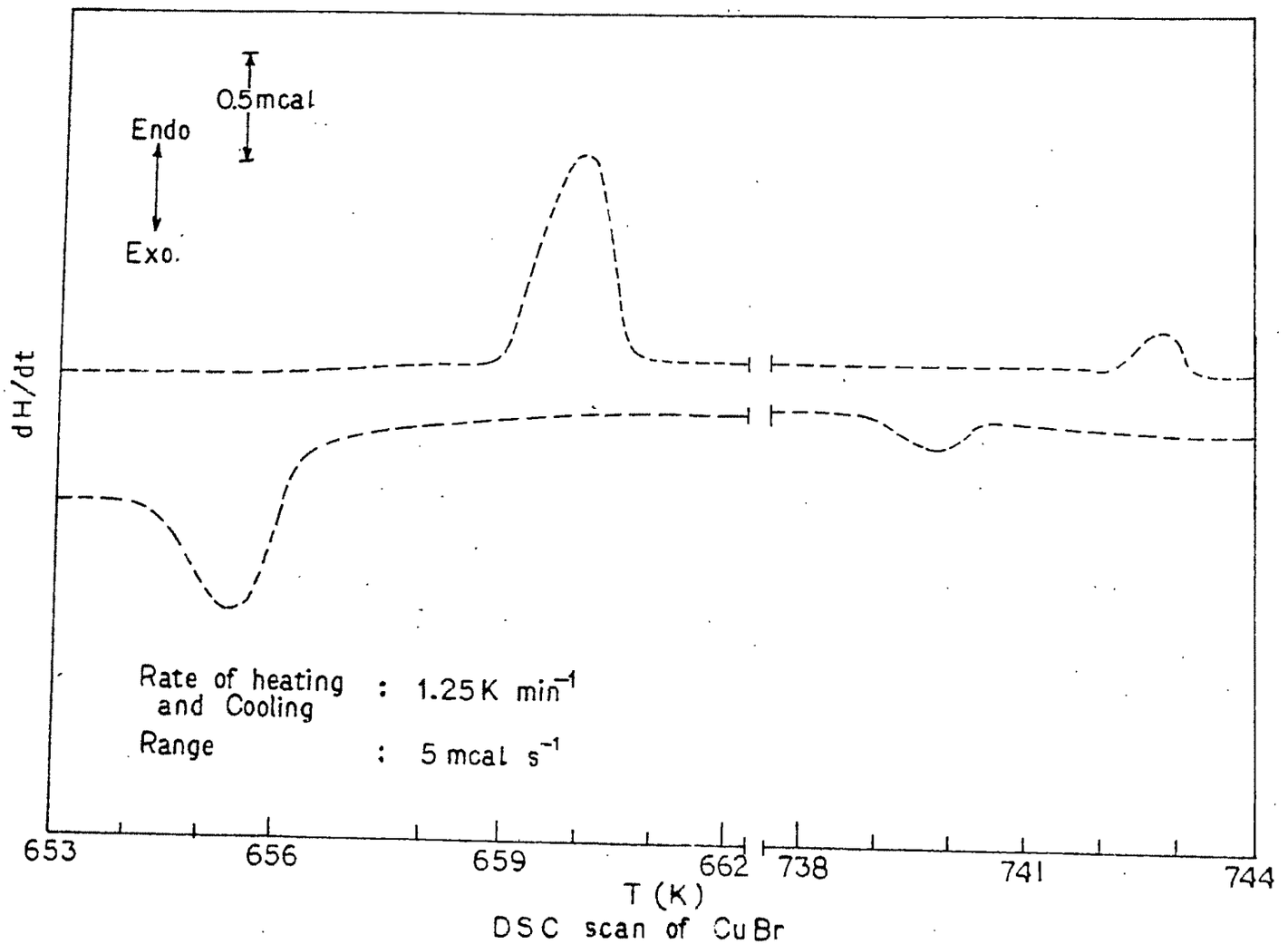

DSC scan of CuBr

Figure. 6.2

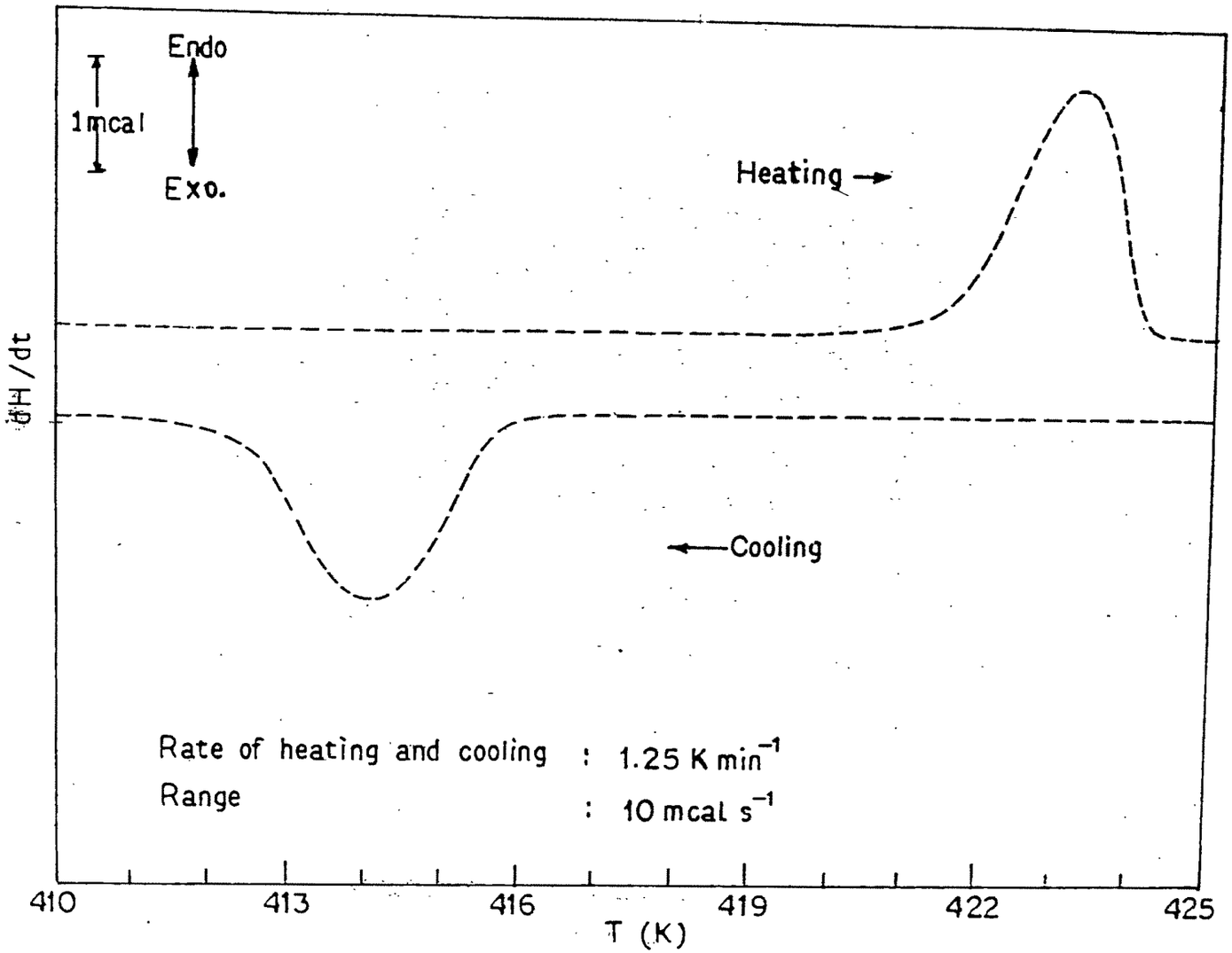

DSC scan of AgI

Figure 6.3

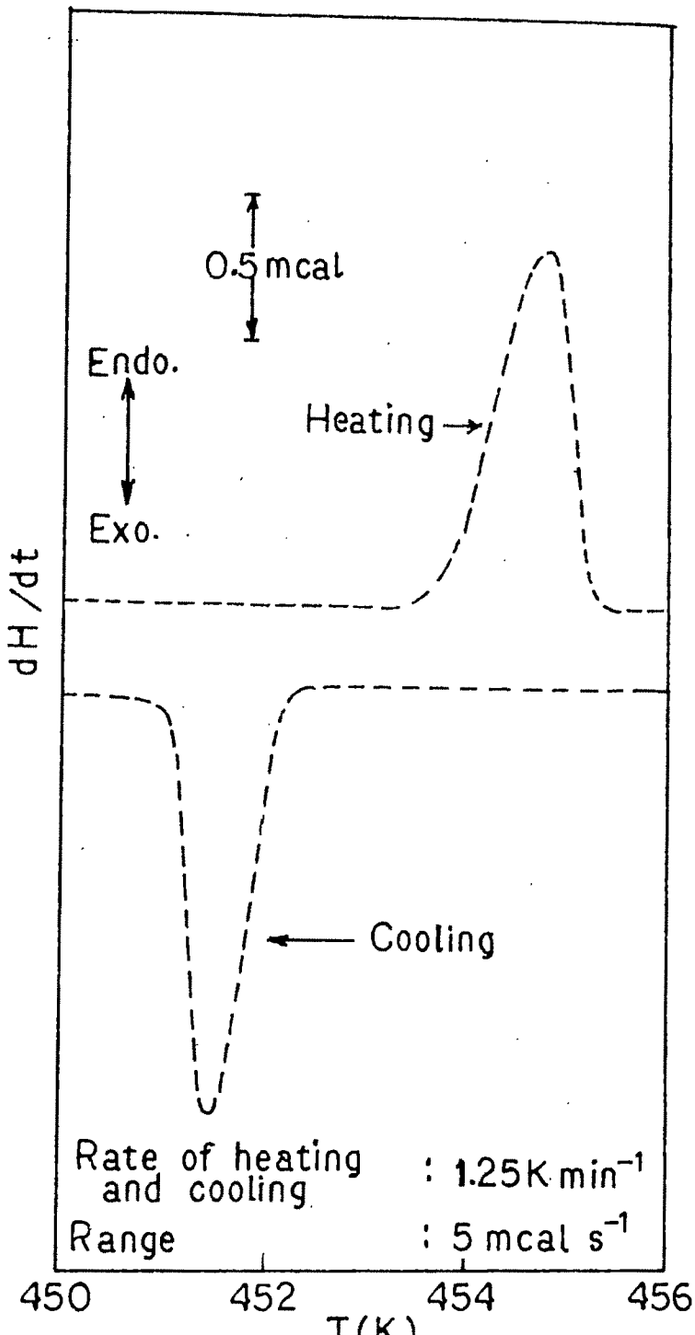

D S C scan of Ag_2S

Figure 6.4

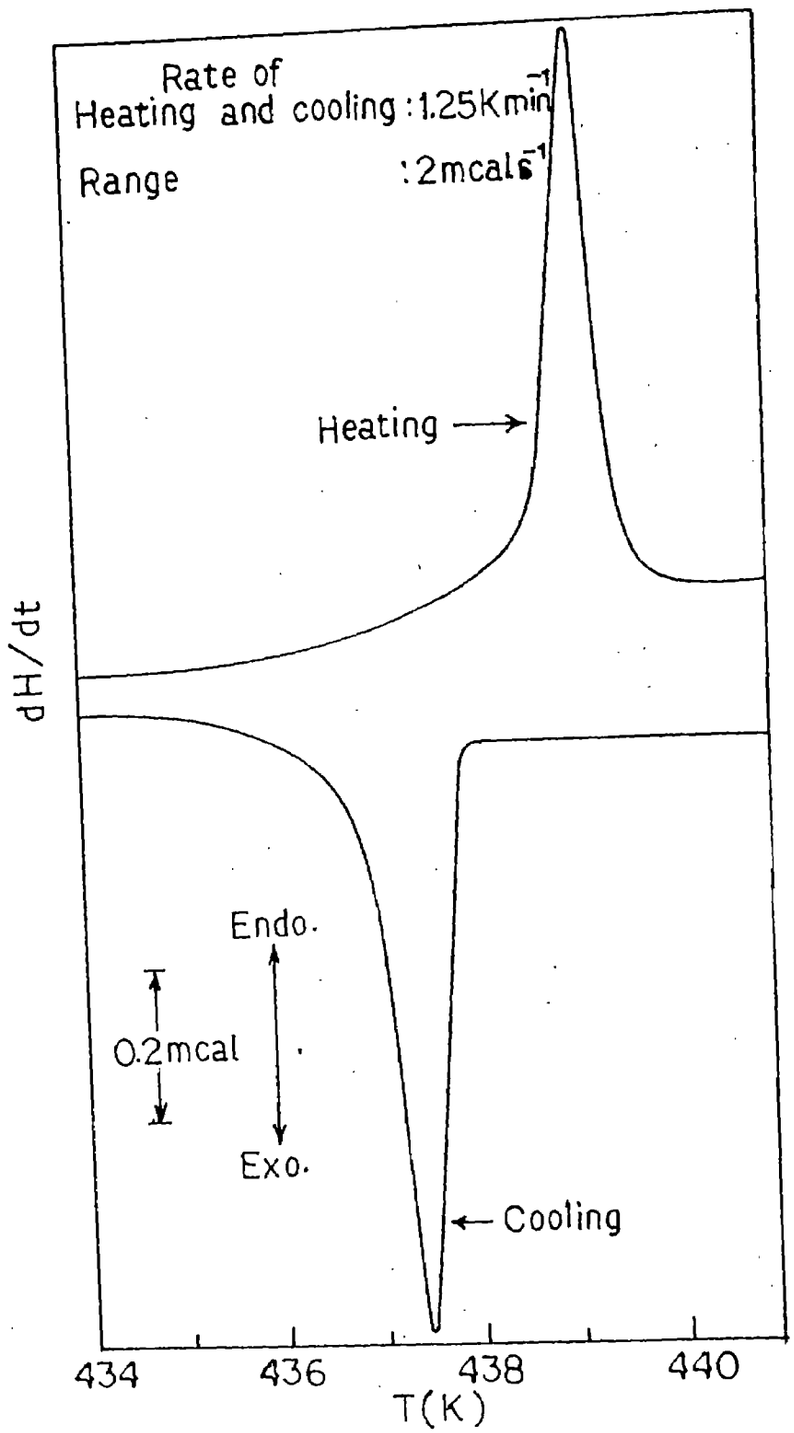

DSC scan of $NaNo_2$

Figure 6.5

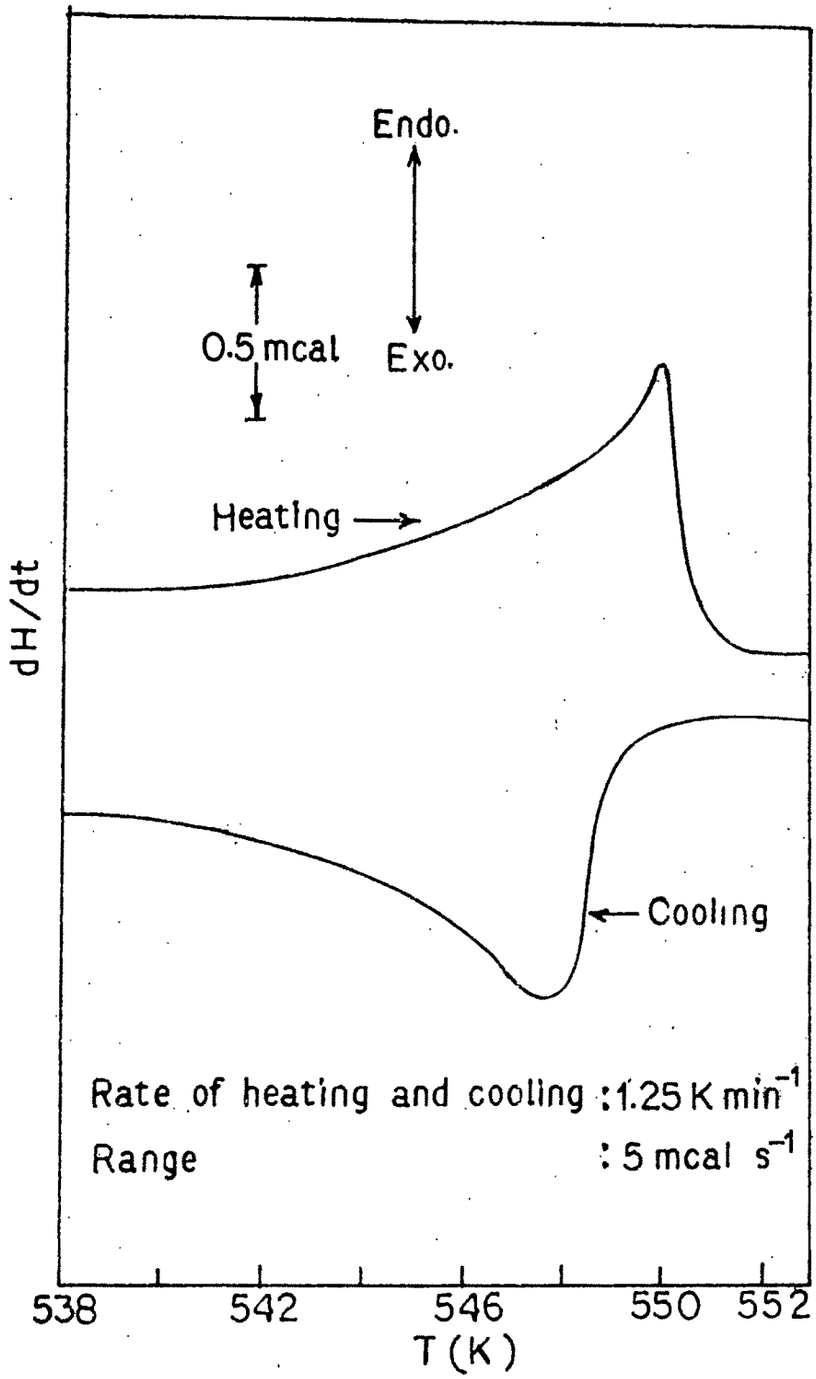

DSC scan of $NaNo_3$

Figure 6.6

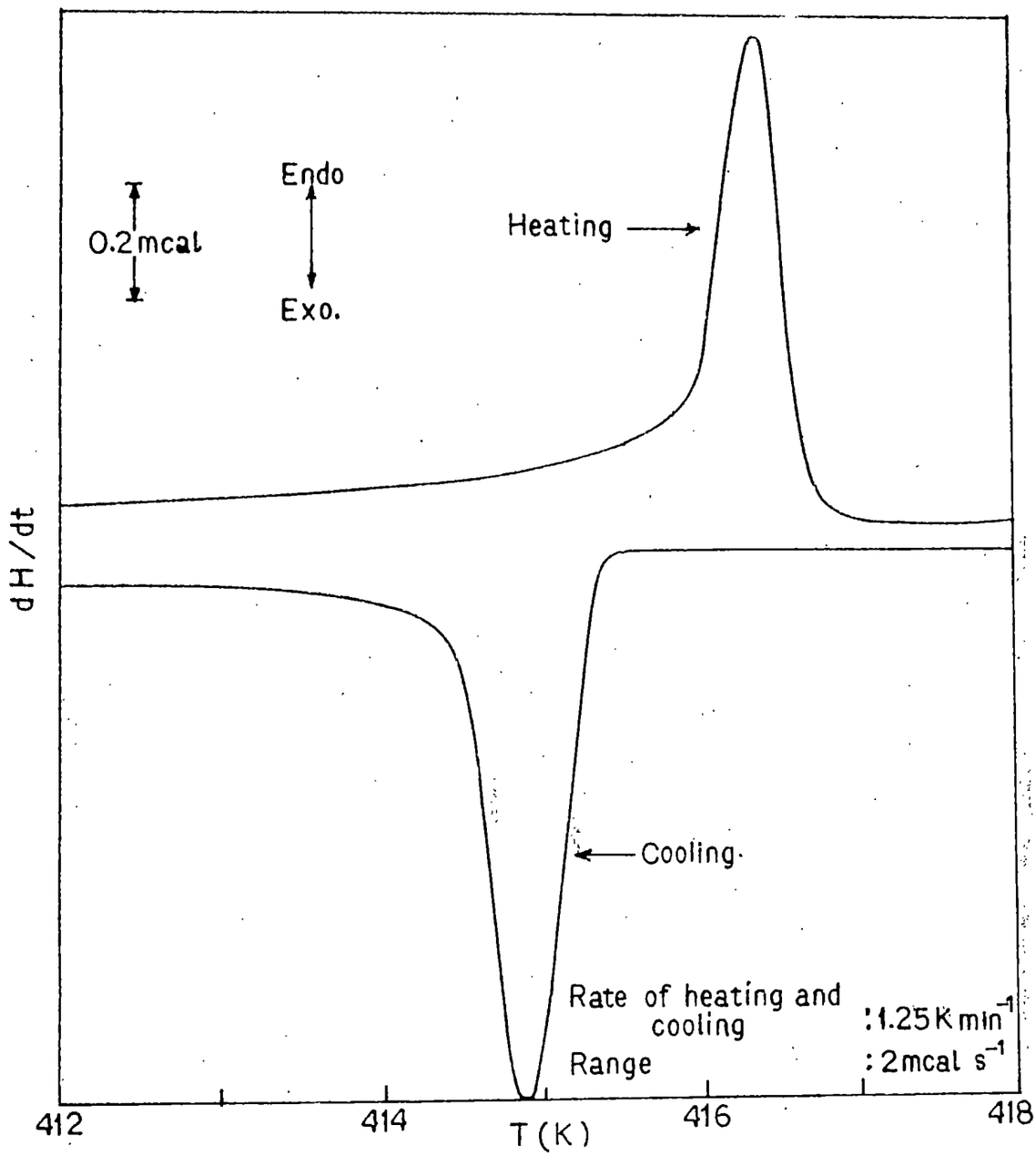

DSC scan of KSCN

Figure. 6.7

Table 6.3

Transition temperatures observed during heating and cooling cycles for the compounds

Compound	Heating[a,b]					Cooling[a,c]				
	Transition	Temperature (K)				Transition	Temperature (K)			
		T_i	T_f	T_m	(T_f-T_i)		T_i	T_f	T_m	(T_f-T_i)
CuI	$\gamma \rightarrow \beta$	646.80	649.40	648.50	2.60	$\beta \rightarrow \gamma$	641.30	633.40	639.20	7.90
	$\beta \rightarrow \alpha$	670.00	672.50	671.20	2.50	$\alpha \rightarrow \beta$	670.90	688.75	669.20	2.15
CuBr	$\gamma \rightarrow \beta$	658.85	661.20	660.00	2.35	$\beta \rightarrow \gamma$	656.70	653.70	655.40	3.00
	$\beta \rightarrow \alpha$	742.00	743.40	742.80	1.40	$\alpha \rightarrow \beta$	740.70	738.80	739.80	1.90
AgI	$\beta \rightarrow \alpha$	420.25	424.40	423.25	4.15	$\alpha \rightarrow \beta$	416.50	410.80	414.10	5.70
Ag_2S	$\beta \rightarrow \alpha$	453.10	455.40	454.10	2.30	$\alpha \rightarrow \beta$	452.50	450.00	451.50	2.50
$NaNO_2$	$\beta \rightarrow \alpha$	435.50	440.00	439.10	4.50	$\alpha \rightarrow \beta$	437.80	434.70	435.40	3.10
$NaNO_3$	$\beta \rightarrow \alpha$	541.00	551.80	550.00	10.80	$\alpha \rightarrow \beta$	550.50	539.30	547.60	11.20
KSCN	$\beta \rightarrow \alpha$	414.20	417.00	416.30	2.80	$\alpha \rightarrow \beta$	412.50	415.50	414.80	3.00

[a] Rate of heating and cooling 1.25 k min^{-1}. [b] Endothermic change. [c] Exothermic change.

This is the general trend observed for order-disorder transition in both positional and orientational types. From this observation it may be concluded that the rate of disordering (during heating) is faster than ordering (during cooling). Attempt was made to determine the relaxation time (τ) for disordering and ordering by using equation of the type (6.2). Although the magnitude of τ obtained for disordering were in general considerably less than in ordering, however, we do not want to attach much significance on it. This is because while using the eqn (6.2) we assumed that the relaxation time is independent of temperature, which, however, is not the case (also see Introduction).

Table 6.4 summarizes the latent heat (ΔH), change in volume of the unit cell (ΔV) and width of hysteresis loop (ΔT) on phase transformation. Comparison of the ΔH values as obtained by us (Table 6.4) with those reported in literature (Table 6.1-6.2) reveal that for AgI and Ag_2S our values are in good agreement with the reported values. However, for the remaining compounds considerable discrepencies exist. It may be pointed out that the transition temperatures reported in literature often differ significantly. Apart from the accuracy of temperature measurements, differences may arise due to variation of heating rates. We have examined this aspect for Ag_2S. Figure 6.8 shows the heating and cooling curves for

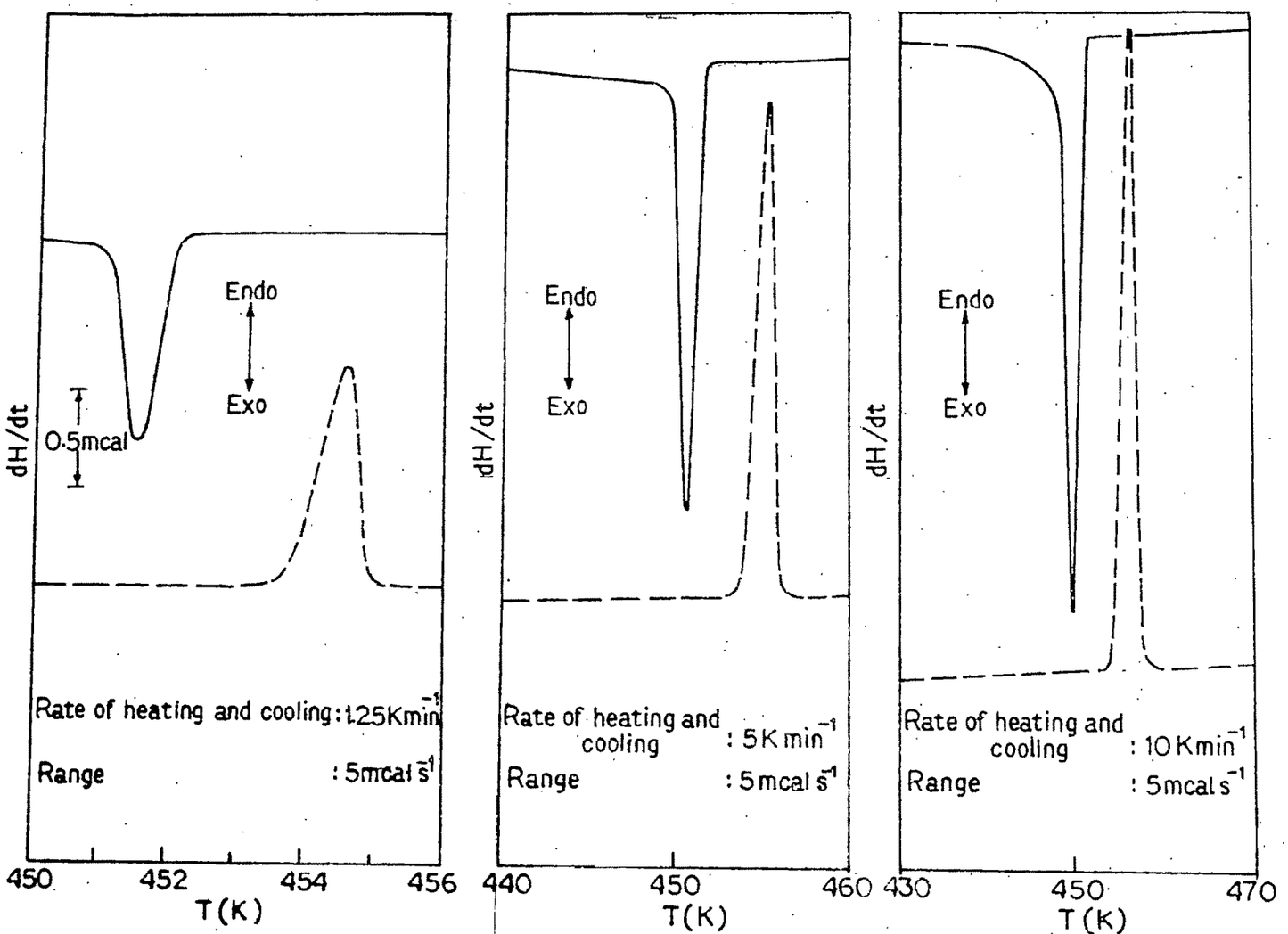

DSC scan of Ag_2S

Figure 6.8

Table 6.4

Latent heat (ΔH), change in volume of unit cell (ΔV) and width of hysteresis (ΔT) on phase transitions

Compound	ΔV ($A^{o\,3}$)	ΔT (^oC)	ΔH (kcal/mol)	
			Heating	Cooling
CuI	2.3 ($\alpha \rightarrow \beta$)	9.3	1.22	1.13
	2.7 ($\beta \rightarrow \alpha$)	2.0	0.16	0.19
CuBr	2.8 ($\gamma \rightarrow \beta$)	4.6	1.17	1.10
	-0.2 ($\beta \rightarrow \alpha$)	2.2	0.27	0.26
AgI	5.9 ($\beta \rightarrow \alpha$)	9.1	1.51	1.50
Ag_2S	7.0 ($\beta \rightarrow \alpha$)	3.5	0.84	0.81
$NaNO_2$	4.4 ($\beta \rightarrow \alpha$)	3.7	0.29	0.30
$NaNO_3$	0.49 ($\beta \rightarrow \alpha$)	2.4	0.40	0.44
KSCN	-	12.3	0.37	0.38

this compound and the related temperatures are collected in Table 6.5. It may be noted that with the increase in heating rates T_m shifts slightly to higher temperature and the width of hysteresis also increases. Thus thermal hysteresis observed in a first order transition will depend upon the rate of heating and cooling. This is a consequence of the variation in kinetics of phase transition with the change in heating/cooling rates. The kinetic aspect is rather involved as the rate process is determined both by nucleation and propagation steps.

Although the free energies of the two phases become equal at the transition temperature, the new phase cannot nucleate due to the existence of kinetic barriers. The nucleation barrier will be higher for transitions involving larger change in volume (ΔV)[1]. For transformation involving a positive ΔV, which usually is the case, the width of hysteresis (ΔT) can be expected to be a function of ΔV.

Observation of hysteresis suggests that the transformation does not occur at the point where the free energies are exactly equal. In the narrow range of temperature where the two phases coexist as a hybrid crystal the free energy surfaces G_1 and G_2 get smeared out and gives rise to a situation as in second or higher order transformations[41]. In the hybrid crystal it is necessary to take into consideration the strain energy (ξ) and interfacial energy (η). Thus at the smeared out

Table 6.5

Transition temperatures of Ag_2S at variable heating/cooling rates

Rate of heating/cooling (k min^{-1})	T_m[a] (K)		Width of hysteresis
	Heating	Cooling	
1.25	454.6	451.5	3.1
5	455.75	450.5	5.25
10	456.5	449.5	7

[a] Peak temperature.

region the free energies of the two phases are

$$G_I = G\ (P,\ T, \xi_{12}, \eta_{12})$$

$$G_{II} = G\ (P,\ T, \xi_{21}, \eta_{21})$$

The strain energy (ξ) is less than breaking strength of the hybrid crystal and the internal surface energy (η) is less than activation energy for self-annealing[41].

Inspection of ΔV and ΔT values in Table 6.4 do not show a definite trend. The notion of ΔT as a function of ΔV will be applicable for compounds having identical crystallographic features. For compounds of variable structures kinetic barriers will be different and therefore strain and interfacial energies will be differently related. This leads us to conclude that no meaningful prediction can be made for thermal hysteresis in compounds of unrelated structures.

REFERENCES

1. C.N.R. Rao and K.J. Rao, "Phase Transitions in Solids", McGraw-Hill Inc., 1978.
2. N.G. Parsonage and L.A.K. Stavely, "Disorder in Crystals", Oxford University Press, 1977.
3. M.A. Krivogalz and A. Smirnov, "The Theory of Order-Disorder in Alloys", Macdonald, London, 1964.
4. H. Yamouchi and D. de Fontaine, in "Order-Disorder Transformation in Alloys", ed. H. Warlimont, Springer-Verlag, Berlin, 1974.
5. J. M. Cowley, J. Appl. Phys., 21, 24 (1950).
6. S. Miyake, S. Hoshino and T. Takenaka, J. Phys. Soc. Jpn., 7, 19 (1952).
7. J. B. Wagner and C. Wagner, J. Chem. Phys., 26, 1597 (1957).
8. W. Buhrer and W. Halg, Electrochimica Acta, 22, 701 (1977).
9. J.B. Boyce, T.M. Hayes and J.C. Mikkelsen, Phys. Rev. B, 23, 2876 (1981).
10. H. Hayashi, J. Phys. Soc. Jpn., 51, 811 (1982).
11. R. Batchelor and T. Birchall, Acta Crystallogr., B38, 1260 (1982).

12. S. Hoshino, J. Phys. Soc. Jpn., 7, 560 (1952).

13. B.R. Lawn, Acta Crystallogr., 17, 1341 (1964).

14. S. Hoshino, J. Phys. Soc. Jpn., 12, 315 (1957).

15. H. Hoshino and M. Shimoji, J. Phys. Chem. Solids, 33, 2303 (1972).

16. H. Hoshino and M. Shimoji, J. Phys. Chem. Solids, 35, 321 (1974).

17. W. Buhrer and W. Halg, Helv. Phys. Acta, 47, 27 (1974).

18. R.W.G. Wyckoff, Crystal Structure, Vol.1, p.110, Interscience (1963).

19. A.J. Fruch Jr., Z. Krist., 110, 136 (1958).

20. C.M. Perrott and N.H. Fletcher, J. Chem. Phys., 50, 2344 (1969).

21. W. Jost and P. Kubaschewski, Z. Physik Chem. N.F. 60, 69 (1968).

22. S. Sawada, S. Nomura, S. Fujii and I. Yoshida, Phys. Rev. Lett., 1, 320 (1958).

23. S. Hoshino, J. Phys. Soc. Jpn., 19, 140 (1964).

24. M. Sakiyama, A. Kimoto and S. Seki, J. Phys. Soc. Jpn., 20, 2180 (1965).

25. I. Hatta and A. Ikushima, J. Phys. Chem. Solids, 34, 57 (1973).

26. S. Hoshino and H. Motegi, Jpn. J. Appl. Phys., 6, 708 (1967).

27. W. Buchheit, G. Herth and J. Petersson, Solid State Commun., 40, 411 (1981).

28. S. Kh. Escryan and V.V. Lemanov, Sov. Phys. Solid State, 23, 1195 (1981).

29. F.C. Kracek, J. Am. Chem. Soc., 53, 1183 (1931).

30. F.C. Kracek, J. Am. Chem. Soc., 53, 2609 (1931).

31. D.M. Newns and L.A.K. Staveley, Chem. Rev., 66, 267 (1966).

32. R.W.G. Wyekoff, "Crystal Structures", Vol. II, Interscience, New York, N.Y., 1948, Section VII.

33. H.P. Klug, Z. Krist., 85, 214 (1933).

34. R. Savoic and Mezolet, Can. J. Chem., 45, 1677 (1967).

35. M. Sakiyama, H. Suga and S. Seki, Bull. Chem. Soc. Jpn., 36, 1025 (1963).

36. Y. Yamada and T. Watanabe, Bull. Chem. Soc. Jpn., 1032 (1963).

37. Z. Iqbal, L.H. Sharma and K.D. Moller, J. Chem. Phys., 57, 4728 (1972).

38. R.N. Keller and H.D. Wycoff, Inorg. Synth., 2, 1 (1946).

39. G.D. Kauffman and R.P. Pinnell, Inorg. Synth., 6, 3 (1960).

40. K. Nag and S. Geller, J. Electrochem. Soc., 128, 2670 (1981).

41. A.R. Ubbelohde, Quart. Rev., 11, 246 (1957).